Traction and Charging Systems for an Electric Motorcycle

Jorge Carvalho, Tiago J. C. Sousa, and Delfim Pedrosa[(⊠)]

Centro ALGORITMI, University of Minho, Campus de Azurém, Guimarães, Portugal
dpedrosa@dei.uminho.pt

Abstract. Low energy consumption vehicles such as Electric Motorcycles (EMs) are a very viable solution to reduce energy consumption in the transportation sector. Due to their low power and weight, EMs have high energy efficiency and are optimized for urban transit. In this context, it becomes necessary to develop systems prototypes for any type of Electric Vehicles (EVs). Therefore, the focus of this paper is the implementation of traction and charging systems for an EM. The traction system is composed by a DC motor and a power converter that operates the motor. The power converter control allows the motor to operate in different modes. Besides, the traction system's input is a hand accelerator/brake that can control the motor speed/torque. The charging system acts as an interface between the power grid and the motorcycle system. With this, the first stage of the charger is AC-DC rectification that, besides regulating the DC-link voltage, should also act as a Power Factor Corrector (PFC) and consume a sinusoidal current from the power grid. The charger should also ensure the battery's safety and offer the possibility of regulating the charging rate. This paper details the development of traction and charging systems from the presentation of topologies to the computational simulations, and respective experimental tests and validation.

Keywords: Battery charging · Electric motorcycles · Brushed DC motor · Regenerative braking · Torque control

1 Introduction

Internal Combustion Engine (ICE) vehicles, which use fossil fuels as a source of energy, represent most of the existing worldwide on-road vehicles today [1]. The shortage of these non-renewable resources, as well as the environmental impact they bring, are considered as some of the most critical worldwide issues [2].

Electric traction systems also have much higher energy and performance efficiency than their conventional counterparts. On top of that, electrified vehicles offer performance advantages such as higher responsiveness, i.e., faster acceleration [1]. With this, electrification of transportation is a paradigm shift, and it is one of the most promising solutions to achieve the global goal of reduced and cleaner energy consumption [1, 2].

In regard to Electric Vehicles (EVs) market there are two tendencies. For one, there are models designed for commuting purposes with low battery weight and short-range.

These are lightweight/low-power vehicles and are optimized for low consumption and urban traffic. On the other hand, there are long-range EVs with high-capacity batteries. However, this section of the market has a major disadvantage regarding range compared to ICE vehicles. Other EV disadvantages when contrasted with ICE vehicles are a higher initial cost and time to charge [3].

Considering the limitations and advantages of EVs, a good solution is the use of low-power EVs such as Electric Motorcycles (EMs). EMs have the advantage of having low energy consumption and are optimized for urban driving since they are compact and easy to park [4]. Considering all the advantages of low-power vehicles, EMs prove to be an economic and environment-friendly solution for work commutes in an urban context [4].

To operate an electric motor is necessary the respective controller [5, 6]. In the market, there is a wide range of motor controllers, varying in terms of power, supply voltage, and functionalities. These motor controllers act as an interface for the user to control speed, rotation direction, regulating torque, starting, stopping the motor and it offers protection against overloads and electric faults. The controllers produced for motor applications employ power electronic converters allied with control methods [5, 6]. With this, the EV requires the integration of a motor controller such as described.

For electric motors, by resorting to power electronics it is possible to recover energy during braking. This processing is called regenerative braking [5, 6]. Regenerative braking allows the mechanical energy from the motor's rotation to be converted into electrical energy that is returned to the battery. This process occurs when the brake is applied, the vehicle slows down and the motor works as a generator and thus recharging the battery [7].

The success of EV technology depends on the availability of EV charging stations. To meet this demand, it is necessary to have a solid power grid infrastructure of charging stations. Unidirectional charging is a logical first step because it limits hardware requirements and simplifies interconnection issues [8]. Aside from the interface between the EV system and the power grid, there must be provided charging control for the battery, e.g., keeping track of the charging and discharging rate [8].

EV charging systems can be classified as on-board and off-board [8]. Off-board chargers are the usual charging stations seen in public spaces and are directly connected to the EV batteries. Off-board chargers have their respective power converters placed between the power grid and the EVs. This charging solution is considered a DC charger [8]. On-board chargers, as the name suggests, are integrated in the EV and their topology is based on AC-DC and DC-DC converters [8–10].

This paper proposes and details the implementation of an electric traction system that activates a brushed DC (BDC) motor, as well as an on-board battery charger system for an EM. Both traction and charger systems are connected to a battery and operate independently. The traction system is operated by means of a user input such has a hand accelerator. The battery charging system acts as an interface between the power grid and the battery, providing PFC and charging current regulation The structure of this paper is composed of a brief introduction, covering the EVs state-of-the-art, in Sect. 2 is presented each systems topologies, followed in Sect. 3 by the respective computational

simulations, thereafter, in Sect. 4 is shown the hardware implemented, and lastly the experimental tests and validation of two systems.

2   Traction and Charging Systems

Based on the contextualization presented above, it is presented a two-converter topology for the EM traction and charging systems, as shown in Fig. 1.

The topology is composed by the motor and charger, where both have an interface with the battery. Considering that both motor and charger do not operate at the same time, the topologies are developed independently.

The charger acts as the interface between the power grid and the battery and is composed by two stages: the first stage is the AC-DC converter for DC voltage regulation and power factor correction; the second stage is charger converter, for battery current control. On the other hand, the motor converter is connected directly to the battery and controls the DC motor.
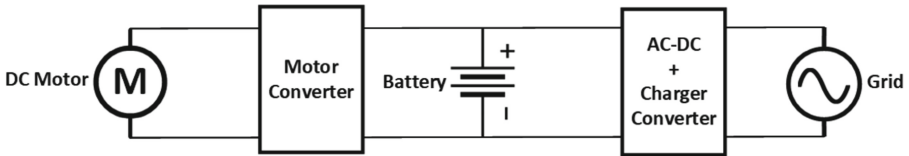

Fig. 1. Presented topology for the implementation of a traction and charging systems using two converters.

2.1   Charger System Topology

For the first stage, the simplest AC-DC converter topology is unidirectional using single-phase diode rectifiers. Usually, the topology used is a Diode Full-Bridge (DFB) that rectifies the grid voltage and producing at the output (DC-link) a constant DC voltage with a certain ripple. The ripple is minimized by the DC-link capacitor, where the ripple is lower with a higher capacitance. On top of those components referred it is also present an inductor after or before the DFB to reduce the power grid current ripple [11]. However, the DFB rectifier has disadvantages such has high effects on the power grid, particularly by absorbing a current with high Total Harmonic Distortion (THD), and an unregulated output voltage that is directly dependent on the power grid voltage level [11].

To achieve a sinusoidal power grid current with THD < 5% (required for the distribution grid), it is opted to implement a Power Factor Corrector (PFC) boost converter, as shown in Fig. 2 [12]. With this, the converter requires two closed-loop controls: one to obtain the reference current for a specific DC-link voltage and the other to regulate the power grid current.

To regulate and control the charging rate and state of the batteries it is required a proper control algorithm. There are diverse charging methods that improve charging safety and regulation, such as the Constant-Current Constant-Voltage (CC–CV) charging method [13]. However, the essential parts of battery chargers are controlling the

charging current while regulating the battery conditions, such as State of Charge (SoC) and temperature [14].

Regarding the type of battery used, the most common for EV applications are lithium-ion (Li-ion) batteries [10]. Li-ion batteries are well suited for transportation applications, due to their high energy/power density ratio, slow self-discharge, and high life cycle [15].
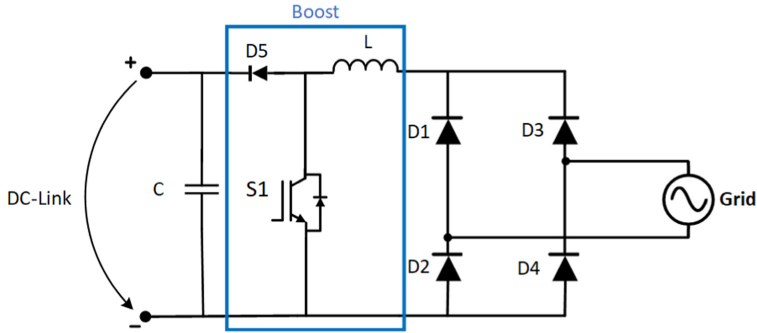

Fig. 2. Electric schematic of the PFC boost rectifier (DFB rectifier + DC-DC boost).

To implement a battery charger, it is required a power converter, and considering that the EV system operates in DC, the options are DC-DC converters. With this, it is implemented a DC-DC buck converter connected to the DC-link resulting in the schematic presented in Fig. 3.
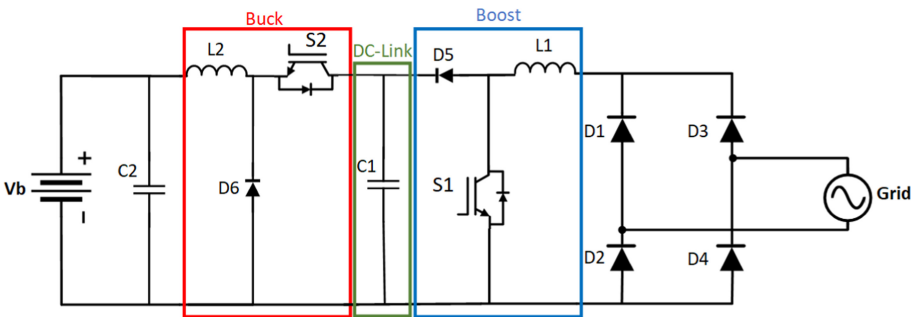

Fig. 3. Electric schematic of the overall charger topology for grid-battery interface.

2.2 Traction System Topology

The motor used in the context of this paper was a BDC motor, despite AC and DC brushless motors also being viable for traction systems applications.

To operate the BDC motor it is opted for a full-bridge or H-Bridge which allows bidirectional current flow, supplies a controllable voltage to a load, and it is constituted by four semiconductors in an H-shape. In Fig. 4 is shown the H-bridge topology, with the

equivalent model of a DC motor being supplied by the battery (V_b). The operation of an H-bridge is based on which semiconductors are active, determining a specific operation mode [7, 16]. Considering this, it is possible to reverse the voltage applied to the load and control the current direction, consequently inverting the motor's rotation. Translating to the context of an EV, the H-bridge controls the operation modes, representing acceleration and braking in both directions (forward and reverse), making up to a total of four functioning modes [16].
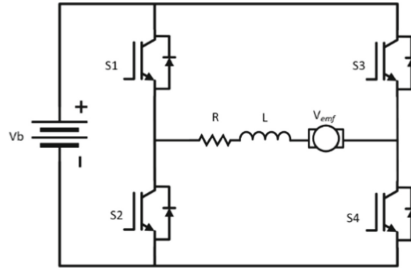

Fig. 4. H-bridge electric schematic applied to the equivalent model of a DC motor, supplied by a battery (V_b).

By observing Fig. 4 it is concluded that each combination of two operating IGBTs define a specific mode. However, both semiconductors of the same leg (S1 and S2 or S3 and S4) cannot be active at the same time, otherwise causing a short circuit. On the other hand, if the two top or two bottom semiconductors are active, the motor coasts and it is idle. Therefore, the remaining four combinations are the most relevant, which define the motor operation. In Table 1 are presented the conditions of each IGBT regarding the four operation modes [16]. The semiconductors can have three states, either fully closed (ON), fully open (OFF) or activated by a PWM wave at the respective gate.

Regenerative braking occurs when it is applied a torque in opposition to the current rotation and the current flows from the motor to the batteries.

Table 1. Motor operation modes and the corresponding combinations of IGBT states.

	S1	S2	S3	S3
1-Forward Motoring	PWM	OFF	OFF	ON
2-Forward Regeneration	OFF	PWM	OFF	ON
3-Reverse Motoring	OFF	ON	PWM	OFF
4-Reverse Regeneration	OFF	OFF	OFF	PWM

For each mode, the motor voltage (V_m) is given by the following equations:

$$V_m = V_b \alpha_1 \tag{1}$$

$$V_m = V_b(1 - \alpha_2) \tag{2}$$

$$V_m = -V_b\alpha_3 \tag{3}$$

$$V_m = -V_b(1 - \alpha_4), \tag{4}$$

where $\alpha_{1,2,3,4}$ correspond to the PWM duty-cycle applied to the respective semiconductor (1-Forward Motoring, 2-Forward Regeneration, 3-Reverse Motoring, 4-Reverse Regeneration).

On top of that, the back-EMF (V_{emf}), which is the speed-induced voltage of the motor, is given by equation:

$$V_{emf} = km\,v, \tag{5}$$

where km is a motor constant and v the motor rotation speed (rpm).

3 Simulations of the Traction and Charging Systems

A simulation tool allows testing the performance of control systems, as well as manipulate their parameters to obtain the desired behavior. Therefore, it is convenient that the used simulation model is very close to the actual model, and to consider non-ideal aspects of the system components. Besides, problems resulting from design errors can be identified and corrected, thus avoiding damage to electronic components.

All presented simulations were performed using PowerSim Inc's PSIM v9.0.3 simulation software, which is especially suitable for power electronics applications.

3.1 Traction Operation

To simulate the traction system, it is required to simulate the equivalent model of the BDC motor used. With this, in Table 2 are presented the most relevant characteristics of the Motenergy ME1003 BDC motor.

Regarding the traction control, it is used a torque control, since it is more intuitive for a user to operate the motorcycle, similarly to a regular vehicle. With this, the motorcycle speed is controlled indirectly by the torque given by the user input (Fig. 5).

The controller allows an accurate torque control proportional to the current applied on the motor. This control is identical to that of the vehicle with a hand accelerator, where it is given an acceleration reference by means of demanding current [7, 16]. It is important to note that the motor torque is directly proportional to the respective current. The control of the BDC motor is based upon the identification of the respective operation mode. For that, it is required to measure the back-EMF and the motor current (i_m) [17]. After defining the conditions for each mode, it is applied a PI current control that generates a control output u [18].

This value is based on the error between the reference current (i_{ref}), given by the user, and the motor current [16]. With this, for each mode, it is obtained:

Table 2. Technical data of the BDC motor simulated.

Characteristics	Values
Electric Power	15 kW
Armature Resistance	0.012 Ω
Armature Inductance	0.93 mH
Rated Voltage	72 V
Rated Current	200 A
Rated Speed	3000 rpm
Voltage Constant	0.0207 V/rpm
Torque Constant	0.197 Nm/A

Mode 1:

If $i_m \geq 0$ and $V_{emf} \geq 0$, then $\alpha_1 = \frac{1}{V_b} (u + V_{emf})$

Mode 2:

If $i_m < 0$ and $V_{emf} \geq 0$, then $\alpha_2 = 1 - \frac{1}{V_b} (u + V_{emf})$

Mode 3:

If $i_m < 0$ and $V_{emf} < 0$, then $\alpha_3 = -\frac{1}{V_b} (u + V_{emf})$

Mode 4:

If $i_m \geq 0$ and $V_{emf} < 0$, then $\alpha_4 = 1 + \frac{1}{V_b} (u + V_{emf})$
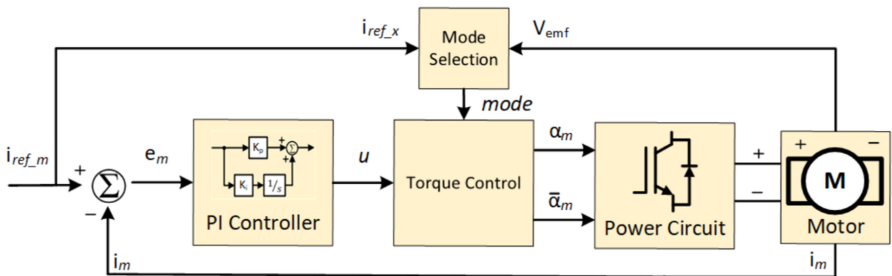

Fig. 5. Block diagram of the traction system torque control.

After implementing the simulation design, it is proceeded to the respective validation. To validate the correct operation of the torque control, the traction system is tested supplied with a 72 V fixed power supply and a 20 Nm mechanical load. On the other hand, to simulate the user input various reference currents are given throughout the simulation, displaying the different modes of operation (Fig. 6 (c)). That being said, in Fig. 6 (a) and Fig. 6 (b) the evolution of mechanical and electrical characteristics are presented, respectively. Observing Fig. 6 (a), from 0 s and 1 s it is possible to confirm that the acceleration/deceleration is proportional to the absolute current value. For the first 0.5 s the motor accelerates with a current of 130 A reaching 1500 rpm, then it is applied the braking, switching to regeneration mode, until speed direction is inverted, causing the motor to accelerate in the opposite direction.

From 0.88 s to 1 s and 1 s to 1.12 s the speed evolution is greater because in those instances the load is applying force in the same direction as the motor, helping decelerate/accelerate as observed in Fig. 6 (b). Transitioning to a practical situation, it is like braking on an uphill or accelerating in a downhill, where in these cases the mechanical load applies torque in the same direction of the motor, increasing acceleration. With this, it is possible to validate the traction system by comparing the intervals of each mode with the evolution of torque and speed, respectively.
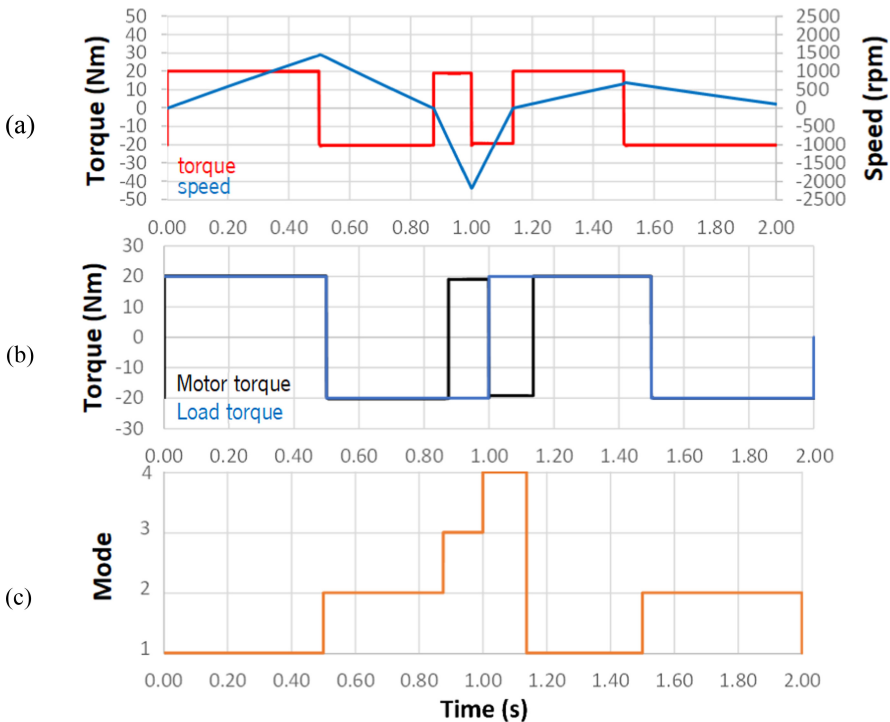

Fig. 6. Motor simulation results with a fixed 72 V power supply: (a) Mechanical characteristics of the motor, speed, and torque; (b) Relation between the torque developed by the motor (motor torque) and the attached load; (c) Motor operation modes from 1 to 4.

To further validate the regenerative braking, it is used the equivalent model of a battery. The battery model is a 2nd order Thevenin circuit. Figure 7 shows the waveforms of the motor current, back-EMF (Fig. 7 (a)) and the battery voltage (Fig. 7 (b)) that can be correlated with the battery SoC.

By observing Fig. 7 (a) it can be validated that during motoring mode the battery is discharged and during braking mode the battery recharges. It is also possible to conclude that, for a greater current, the battery voltage varies faster, as predicted.

3.2 Charging Operation

The requirements set for the AC-DC converter are 3 kW rated power and a DC-link voltage of 400 V. Considering the converter has an input voltage of 230 V (RMS), the rated absorbed grid current (i_g) is 13.05 A (RMS).

The AC-DC converter implemented in simulation is the passive PFC boost topology with a PI current control technique. In this control strategy, the DC-link voltage (V_{dc}) is measured and compared to the reference value ($V_{dc.ref}$), resulting in an error signal ($V_{dc.error}$), that it is subjected to a PI controller. The output of the PI controller is a reference current (i_{ref}), used for the PFC current control. For the proper operation of the AC-DC converter it is necessary to synchronize the system with the power grid voltage. Therefore, it is used a Phase-Locked-Loop (PLL) algorithm, which generates a sinusoidal signal that is an input for the PFC current control.
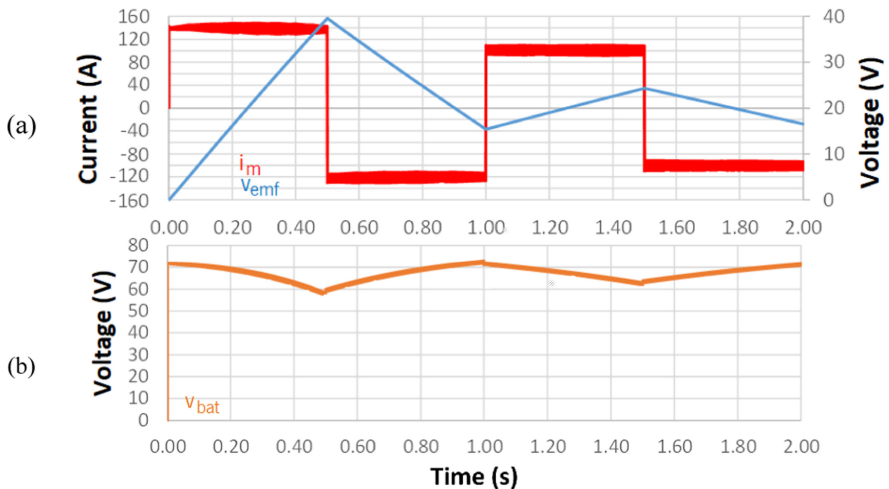

Fig. 7. Motor simulation results with a 72 V battery: (a) Represents the input reference current and the back-EMF voltage produced by the motor; (b) Corresponds to battery voltage evolution throughout the simulation.

Figure 8 presents the simulation results for the AC-DC converter. In this regard, Fig. 8 (a) shows the DC-link voltage active regulation stabilized at 400 V with 20 V of ripple. Figure 8 (b) shows a sinusoidal power grid current with low harmonic content (THD$_f$ of 0.65%) and the current i_{ref} calculated by the DC-link control. With this, it is possible to validate both the DC-link regulation and the PFC current control.

To activate the battery charging control, it is necessary to stabilize the DC-link voltage. Therefore, the buck converter is activated when the input voltage is higher than 390 V. The simulation results of the buck converter are shown in Fig. 9, where are present the reference charging current (i_{ref}) and the battery current (i_{bat}), as well as the battery voltage (v_{bat}).
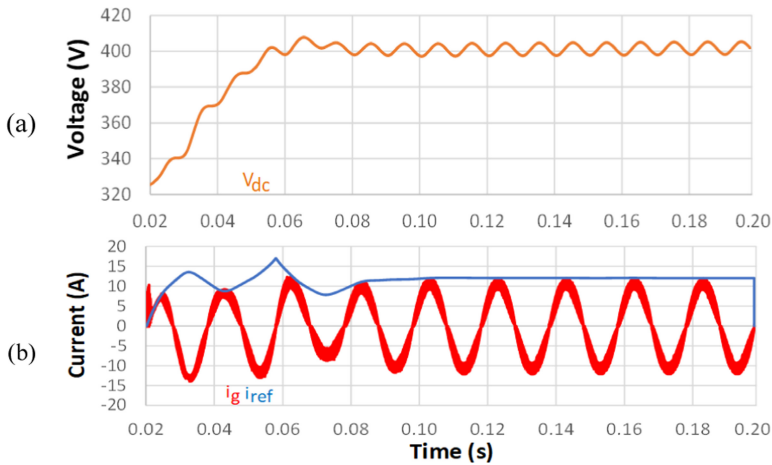

Fig. 8. Simulation waveforms of the AC-DC converter and the respective PFC and DC-link regulation functions.

Figure 9 (a) shows the reference input current and the battery charging current. At the start of the charging process, it is specified a reference current of 20 A, then, at a later stage, this value is lowered to 10 A. Figure 9 (b) shows the battery voltage evolution during the charging process. It is also observable that, during the period of higher current, the battery charges faster concerning the later stage, reaching 80 V. With this, it is possible to confirm the correct functioning of the PI current control.
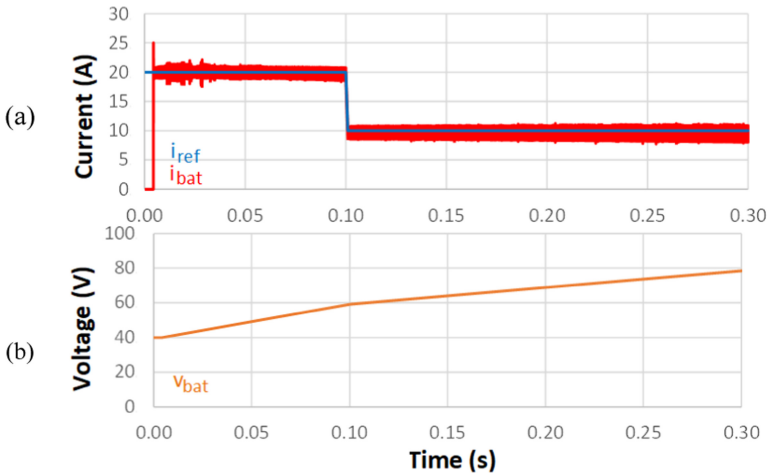
Fig. 9. Simulation waveforms of the buck converter for charging current control: (a) Reference, and battery charging currents. (b) Battery voltage that is correlated with the respective charge.

4 Experimental Tests and Results

The experimental tests conducted are necessary for the development of specific hardware. Therefore, two Printed Circuit Boards (PCBs) were developed. One is a control PCB (Fig. 10 (a)), where signal conditioning of the sensors outputs is performed to be processed by the Analog to Digital (ADC) module of the DSP. The control PCB also has error processing, to detect and act on voltage or current anomalies by turning off the converter's operation, and the driver circuits for the two semiconductors of the charger converters. The other implemented PCB was the charger converter power circuit (Fig. 10 (b)), where are located the semiconductors, DC-link capacitors, voltage and current sensors and the connection to the power grid.

In Fig. 11 is shown the motor traction system, including the control system, where each part is described.

4.1 Traction Operation

For the conducted tests it is used a constant DC power supply of 31 V instead of a battery, therefore the validation of the regenerative braking is conditioned. However, due to the high capacitance on the DC-link input, making up to 10 mF capacitance, it is possible during mode 2 to return energy to these capacitors. This phenomenon is monitored by observing the motor's current direction, which is negative, or rather, from the motor to the capacitor bank. The reference current range used on the tests shown is from −5 A to 15 A, which without a mechanical load the acceleration is already very significant. On top of that tests with a 2 Nm mechanical load were conducted, where the only noticeable differences it is a higher current threshold for the motor to generate enough torque to rotate.
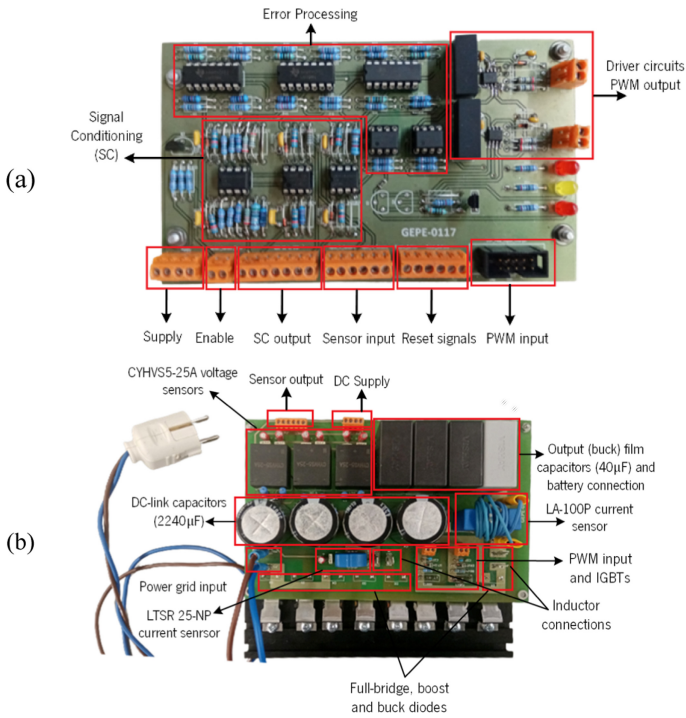
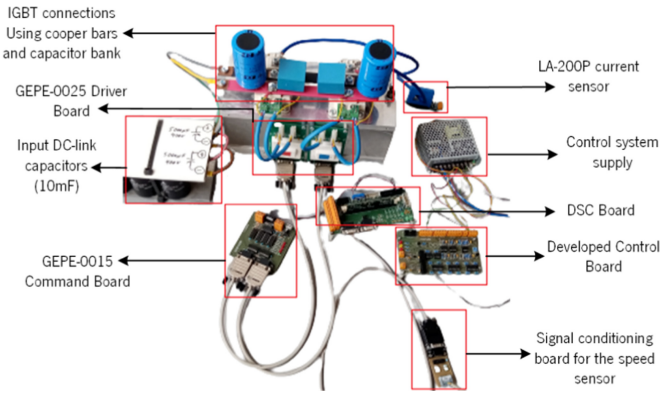**Fig. 10.** Developed PCBs: (a) Control board; (b) Charger power board.

Fig. 11. Traction system assembly and respective connections between PCBs.

Considering the test description above, the motor results are presented in Fig. 12, showing the back-EMF voltage (V_{emf}), the operation mode, the motor current (i_m) and the respective reference (i_{ref}). By observing the waveforms of Fig. 12 it is possible to compare the motor current value with the reference and conclude that the control

is functioning properly, and it has a good reaction time. On top of that can also be established the relation between current/torque and the speed evolution.

4.2 Charging Operation

To test the current control, it was set a power grid voltage of 24 V RMS and a DC-link reference voltage of 40 V (10% of the nominal value). To evaluate the PFC behavior, it was measured the reference current (i_{ref}) and the DC-link voltage (V_{dc}), as well as both power grid voltage and current (V_g and i_g). By measuring these quantities, it is expected to obtain results similar to the waveforms obtained in the simulation. For the experimental tests, a 26 Ω resistive load was used on the output. In Fig. 13 (a) is shown the waveform of the power grid current without the PFC current control. In Fig. 13 (b) the DC-link regulation and PFC current controls are activated, and it is possible to verify that the DC-link voltage value is what was expected (40 V with a ripple of 2 V (5%)). On top of that, it is validated the current control considering that the absorbed current has a THD$_f$ of 5.26%.
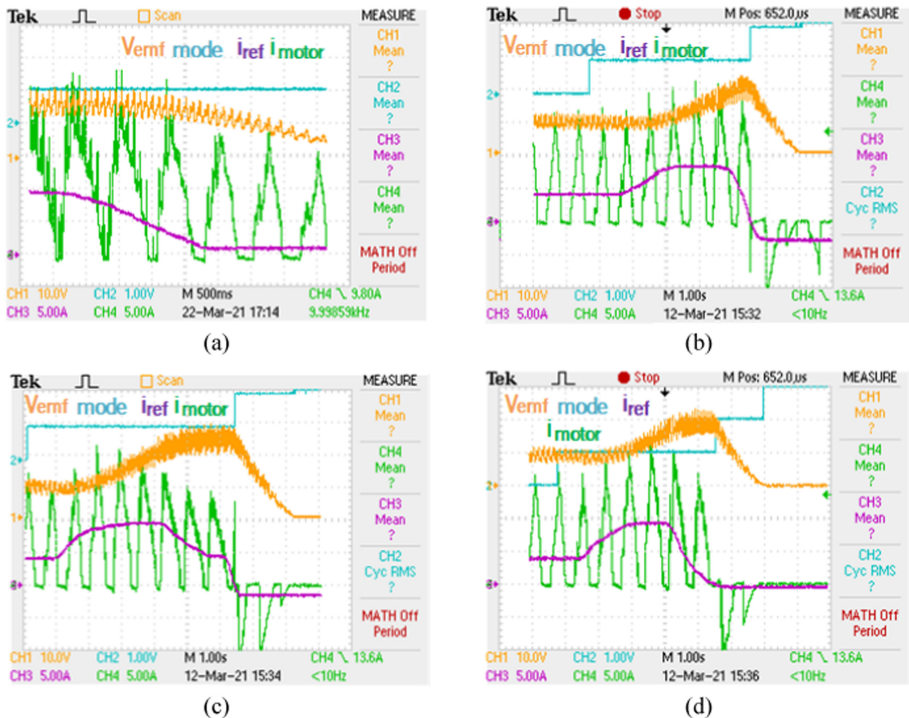

Fig. 12. Waveform results of motor operation showing the waveforms/curves of the back-EMF voltage (CH1: 10 V/div), mode (CH2: modes 0 to 4 (0 no control active) as per established before (1 mode/div)), reference current (CH3: 5 A/div), and motor current (CH4: 5 A/div): (a) Deceleration test while in mode 1; (b) Transition from open loop to control to mode 1 and (c) Acceleration test followed by regenerative braking; (d) Test of modes 1, 2, 3. Time scale of 1 s/div.

To evaluate the PFC behavior, it was measured the reference current (i_{ref}) and the DC-link voltage (V_{dc}), as well as both power grid voltage and current (V_g and i_g). By measuring these quantities, it is expected to obtain results similar to the waveforms obtained in the simulation. For the experimental tests, a 26 Ω resistive load was used on the output. In Fig. 13 (a) is shown the waveform of the power grid current without the PFC current control. In Fig. 13 (b) the DC-link regulation and PFC current controls are activated, and it is possible to verify that the DC-link voltage value is what was expected (40 V with a ripple of 2 V (5%)). On top of that, it is validated the current control considering that the absorbed current has a THD$_f$ of 5.26%.
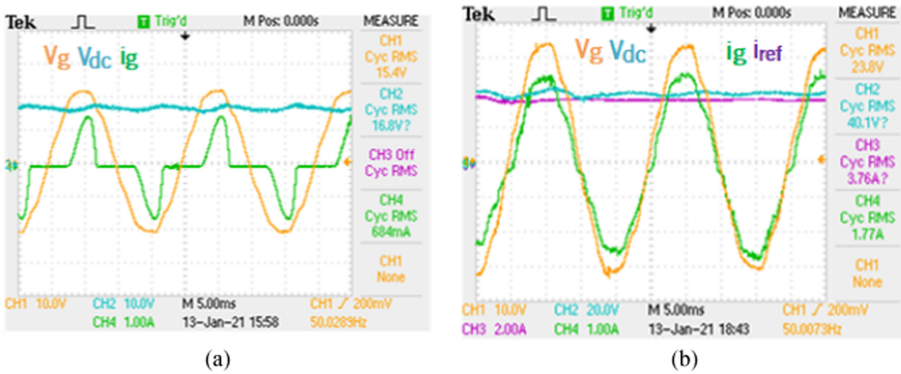

Fig. 13. PFC waveform results: (a) Synthesized current without the current control (CH4: 1 A/div), pre-charge DC-link voltage (CH2: 10 V/div) and power grid voltage (CH1: 10 V/div). Time scale of 5 ms/div; (b) Absorbed power grid current (CH4: 1 A/div), reference current, (CH3: 2 A/div), DC-link voltage (CH2: 20 V/div) and grid voltage (CH1: 10 V/div).

The next step to validate the charging system was the buck converter. With this, considering the stipulated values for the PFC tests, a reference charging current of 1 A is set. On the other hand, during the conducted tests it was used a resistive load instead of a battery, which it is not optimal for validating the charging control. However, it is still possible to confirm the correct implementation of the PI control by setting a fixed reference current. Therefore, it was used a resistive load of 13 Ω, and activated the PFC converter as presented above. Figure 14 shows the charger control in steady-state, where can be seen a constant load current of 1 A. On top of that, it is verified that the DC-link voltage remains stable during charging, and that both PFC and charger controls do not destabilize each other.
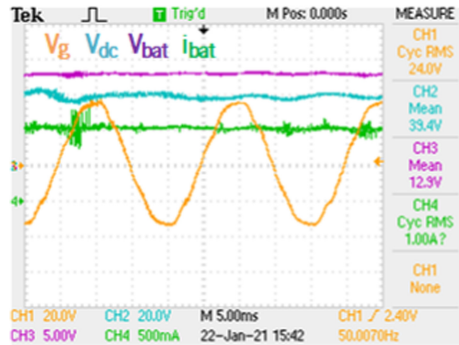
Fig. 14. Buck converter waveform results showing power grid voltage (CH1: 20 V/div), DC-link voltage (CH2: 20 V/div), battery (load) voltage (CH3: 5 V/div) and battery current (CH4: 500 mA/div). Time scale of 5 ms/div.

5   Conclusions

This paper has presented the implementation of traction and battery charging systems for an Electric Motorcycle (EM). Both systems were developed independently and are connected to a battery bank. The traction system is composed by a Brushed DC motor (BDC) and an H-bridge converter that allows four motor operation modes and is supplied by the battery bank. The modes are motoring and regenerative braking, both forward and reverse directions. The control for the traction system is a current/torque control which has a user interface by means of a hand accelerator/brake. The mode transition is performed automatically based on the user's input. The charging system is composed by two stages, where firstly is utilized a PFC boost for AC-DC purposes, to regulate the DC-link voltage while consuming a sinusoidal power grid current. The second stage is composed by a buck DC-DC converter that applies a charging current control for the battery. For the charging system, it is established a 3 kW rated power, with 400 V on the DC-link and a 13 A (RMS) power grid current. The computer simulations and the experimental tests presented allowed the validation of the developed topologies, as well as the hardware implementation.

References

1. Liberto, C., Valenti, G., Orchi, S., Lelli, M., Nigro, M., Ferrara, M.: The impact of electric mobility scenarios in large urban areas: the Rome case study. IEEE Trans. Intell. Transp. Syst. **19**(11), 3540–3549 (2018). https://doi.org/10.1109/TITS.2018.2832004
2. Adib, A., et al.: E-mobility – advancements and challenges. IEEE Access **7**, 165226–165240 (2019). https://doi.org/10.1109/ACCESS.2019.2953020031

3. De Santiago, J., et al.: Electrical motor drivelines in commercial all-electric vehicles: a review. IEEE Trans. Veh. Technol. **61**(2), 475–484 (2012). https://doi.org/10.1109/TVT.2011.217 7873

4. Farzaneh, A., Farjah, E.: a novel smart energy management system in pure electric motorcycle using COA. IEEE Trans. Intell. Veh. **4**(4), 600–608 (2019). https://doi.org/10.1109/TIV.2019. 2938100

5. Boopathi, C.S., Saha, S., Singh, A., Sinha, S.: Regenerative braking in electric vehicles. Int. J. Recent Technol. Eng. **8**(2 Special Issue 11), 3338–3346 (2019). https://doi.org/10.35940/ ijrte.B1562.0982S1119

6. Hsu, Y.C., Kao, S.C., Ho, C.Y., Jhou, P.H., Lu, M.Z., Liaw, C.M.: On an electric scooter with G2V/V2H/V2G and energy harvesting functions. IEEE Trans. Power Electron. **33**(8), 6910–6925 (2018). https://doi.org/10.1109/TPEL.2017.2758642

7. Hasanah, R.N., Andrean, V., Suyono, H., Soeprapto: An effective method of regenerative braking for electric vehicles. Int. J. Adv. Sci. Eng. Inf. Technol. **7**(5), 1943–1949 (2017). https://doi.org/10.18517/ijaseit.7.5.1405

8. Yilmaz, M., Krein, P.T.: Review of battery charger topologies, charging power levels, and infrastructure for plug-in electric and hybrid vehicles. IEEE Trans. Power Electron. **28**(5), 2151–2169 (2013). https://doi.org/10.1109/TPEL.2012.2212917

9. Charger, Q.I.O., Na, T., Zhang, Q., Tang, J., Wang, J.: Active Power Filter for Single-Phase **3**(3), 197–201 (2018)

10. Saber, C., Labrousse, D., Revol, B., Gascher, A.: Challenges facing PFC of a single-phase on-board charger for electric vehicles based on a current source active rectifier input stage. IEEE Trans. Power Electron. **31**(9), 6192–6202 (2016). https://doi.org/10.1109/TPEL.2015. 2500958

11. Kolar, J.W., Friedli, T.: The essence of three-phase PFC rectifier systems part i. IEEE Trans. Power Electron. **28**(1), 176–198 (2013). https://doi.org/10.1109/TPEL.2012.2197867

12. Li, G., Huang, H., Song, S., Liu, B.: A nonlinear control scheme based on input–output linearized method achieving PFC and robust constant voltage output for boost converters. Energy Rep. **7**, 5386–5393 (2021). https://doi.org/10.1016/j.egyr.2021.08.169

13. Liu, H., et al.: An analytical model for the CC-CV charge of Li-ion batteries with application to degradation analysis. J. Energy Storage **29**, 101342 (2020). https://doi.org/10.1016/j.est. 2020.101342

14. Sarrafan, K., Muttaqi, K.M., Sutanto, D.: Real-time estimation of model parameters and state-of-charge of li-ion batteries in electric vehicles using a new mixed estimation model. IEEE Trans. Ind. Appl. **56**(5), 5417–5428 (2020). https://doi.org/10.1109/TIA.2020.3002977

15. Miniguano, H., Barrado, A., Lazaro, A., Zumel, P., Fernandez, C.: General parameter identification procedure and comparative study of Li-Ion battery models. IEEE Trans. Veh. Technol. **69**(1), 235–245 (2020). https://doi.org/10.1109/TVT.2019.2952970

16. Wu, F.K., Yeh, T.J., Huang, C.F.: Motor control and torque coordination of an electric vehicle actuated by two in-wheel motors. Mechatronics **23**(1), 46–60 (2013). https://doi.org/10.1016/ j.mechatronics.2012.10.008

17. Zhang, Q., Wen, B., He, Y.: Rotational speed monitoring of brushed DC motor via current signal. Meas.: J. Int. Meas. Confed. **184**, 109890 (2021). https://doi.org/10.1016/j.measur ement.2021.109890

18. Vidlak, M., Makys, P., Stano, M.: Comparison between model based and non-model based sensorless methods of brushed DC motor. Transp. Res. Proc. **55**(2019), 911–918 (2021). https://doi.org/10.1016/j.trpro.2021.07.059